Solid State Ionics 32/33 (1989) 771–782
North-Holland, Amsterdam

CERAMIC NANOSTRUCTURE MATERIALS, MEMBRANES AND COMPOSITE LAYERS

A.J. BURGGRAAF, K. KEIZER and B.A. VAN HASSEL
Department of Chemical Technology, Laboratory for Inorganic Chemistry, Materials Science and Catalysis, University of Twente, P.O. Box 217, 7500 AE Enschede, The Netherlands

Received 23 May 1988; accepted for publication 24 June 1988

Synthesis methods to obtain nanoscale materials will be briefly discussed with a focus on sol–gel methods. Three types of nanoscale composites (powders, membranes and ion implanted layers) will be discussed and exemplified with recent original research results. Ceramic membranes with a thickness of 1–10 μm consist of a packing of elementary particles with a size of 3–7 nm. The mean pore size is about 2.5–3 nm. The preparation routes are based on sol and sol–gel technologies. The pores can be modified by liquid as well as by gas deposition techniques. This leads to modification of the chemical character and the effective pore size and gives rise to microstructure elements well below the size of the pores (3 nm). The modification of ceramic surface layers with a thickness of 0.05–0.5 μm by ion implantation and annealing procedures yields amorphous or strongly supersatured metastable solid solutions of e.g. Fe_2O_3 (or TiO_2) in zirconia–yttria solid solutions or of very finely dispersed metal particles in the ceramic surface layers. Particle sizes are of the order of 2–4 nm. Both types of structures have interesting transport, catalytic and mechanical properties.

1. Introduction and general considerations

Nanocrystalline materials can be thought of as a polycrystalline state of matter in which the size of the individual crystallites is of the order of 1–50 nm. In some cases these crystallites form the elementary building units of the microstructure, in other cases they form a substructure of ceramic grains.

Characteristic is the large volume fraction of the atoms located in grain boundaries or interfacial regions. In grains with a size of 5 nm and a thickness of the grain boundary region of 1 nm already 50% of the atoms is located in that grain boundary region. In this region the composition, structure (coordination) and chemical binding is different from that of the bulk. Consequently quite different properties must be expected for nanocrystalline materials. This will especially be the case when the microstructural scale is comparable to the physical dimensions that characterise the phenomena (domain size, Debye length in surface region, dimensions of plastic zone around a crack tip), when the property is dependent on a large volume fraction of the interface or on the very small radius of curvature. Some illustrative results are given below.

Recently Gleiter [1] showed that properties like density, specific heat and thermal expansion of metals (Fe, Cu, Ti) are in the nanoscale structure quite different from those in the bulk. Nanoscale composites could be produced in Au–CaF_2, Pb–Al_2O_3 and Au-polyethylene systems.

Some examples of exotic non-additive properties which can be obtained in heterogeneous mixtures are given by Yanagida et al. [2]. A heterogeneous (porous) mixture of (acid) TiO_2 and (basic) $MgCr_2O_4$ is much more sensitive to humidity than each of the components. The same holds for mixtures of CuO and ZnO, the hetero contact points giving the material sensitivity to humidity and selectivity for CO oxidation. Some novel micro- and nano-structures which can be obtained by advanced processing are discussed by Bender et al. [3]. Interesting results are mentioned in some toughened materials with improved mechanical properties (Al_2O_3–MgO–TiO_2, Al_2O_3–SiO_2–TiO_2 and Al_2O_3–ZrO_2). Metastable structures could be obtained from rapid quenching of droplets of the melt phase (obtained by different methods [3] and by ion implantation [4]).

Ceramic membranes with nanoscale structures are reported for monophasic, diphasic and modified

0 167-2738/89/$ 03.50

materials by Burggraaf et al. [5,6] and for xerogels by Komarmeni et al. [7].

In this paper a brief review will be given of the different methods to obtain nanoscale structures in ceramic materials. Some typical results will be mentioned, a more thorough treatment will be postponed to a later paper. The latter sections of this paper will be focused on recent results in ceramic membranes and in ion-implanted layers.

2. Synthesis methods and principles

The most important synthesis methods are summarised in table 1.

Starting with solids, spinodal decomposition of glasses by heat treatment followed by acid leaching results in porous glasses (Vycorglass) with a pore size around 4 nm. This technique is discussed too by Hurt and Viechnicki [8] to initiate the nucleation of a crystalline phase in the synthesis of glass ceramics. For the ZrO_2–Al_2O_3–SiO_2 system a spinodal separation wavelength for the resulting two-phase mixture down to 2.5–5 nm could be obtained.

A second method makes use of ordering reactions in solid solutions resulting in micro (nano) domain formation. Results are discussed by Burggraaf et al. [9] and by Randall et al. [10]. For the ferro electric perovskite structure $Pb(Sc_{0.5}M_{0.5}O_3)$ with M=Nb or Ta the disordered Sc/M sublattice could be ordered by heat treatment starting from domains with a size of about 20 nm which grow during further annealing. Another example is the formation of nanodomains with pyrochlore structure in the oxygen ion conductive fluorite structures $(Tb_xGd_{1-x})_2$- Zr_2O_7 [11]. The domains have an average diameter ranging from a value smaller than 10 nm for $x=0.2$ to 100 nm for $Gd_2Zr_2O_7$. They grow during annealing,

Table 1
Synthesis methods for nanoscale structures.

	Process type	Product
(1) From solids		
1. (spinodal) demixing	(a) leaching	porous glass
	(b) (re)crystallisation	glass ceramic
2. micro (nano) domain formation	ordering reactions by heat treatment	ceramics (electr., mech.)
(2) From gases or melt		
1. chemical decomposition	thermal decomposition of organometallic precursor	ultra fine ceramics and metals
2. nucleation/quenching	evaporation–condensation of powder; compaction	
3. (metastable) crystallisation/ quenching	laser of plasma melting, splat cooling, compaction	
(3) From sols or gels		
1. colloidal packing	gelation of colloidal suspension	single phase and composite:
2. restructuring of gel	(partial) crystallisation of polymeric gel	1) powders 2) monoliths 3) coatings 4) membranes
(4) Modification technologies		
1. porous ultrastructures	impregnation–precipitation in xerogels or ceramics	see 3.1. with modified properties
2. surfaces/interfaces	– ion implantation – segregation	layers with metastable composition and structures

have interesting catalytic properties in oxidation reactions and finally form antiphase boundaries with rapid oxygen diffusion pathways. A second group of methods starts with the nucleation of the new phase in a gas or melt, followed by condensation and/or rapid cooling (quenching). Only a few examples will be given below. In this way Gleiter [1] reports the evaporation/quenched condensation of metal particles followed by cold compaction of the powder. In the case of Ti, the metal is oxidised before compaction. The final oxide compact should have a particle size of 1–10 nm and behave more or less plastically. Interesting results are briefly reported by Bender et al. [12] for powders obtained by splat (or anvil) cooled droplets of ceramic melts, followed by a consolidation treatment. This results in metastable phases and a duplex type of micro (nano) structure for Al_2O_3–MgO–TiO_2, Al_2O_3–SiO_2–TiO_2 and Al_2O_3–ZrO_2 materials. Kalonji [13] reports for the eutectic composition in the Al_2O_3–ZrO_2 system a lamellar structure with a spacing of 15–100 nm. The molten droplets are in these cases obtained by plasma or laser melting of the oxides. In the transformation toughened system ZrO_2–Y_2O_3 a nanoscale substructure is observed within each grain, consisting of the tetragonal prime (T') phase and forming antiphase boundaries and very clean grain boundaries [13].

The third group of methods starts with the synthesis of a colloidal suspension (sol) and/or a gel from which are produced powders, coatings, monolithic xerogels and ceramic membranes by subsequent heat treatment and/or crystallisation. There exist many variations and its importance in the production of advanced ceramics is reflected in the rapidly expanding literature and congress activity [14–17].

The main characteristic of this group of methods is its ability to form very small elementary particles (3–10 nm) which in the liquid are loosely bound in larger aggregates (up to 1 μm). During further (appropriate) processing the aggregates can be broken down and a more or less regular and uniform packing results in powder particles or layers with mean pore sizes down to 2.5 nm. The advantages of the method are tabulated below and include the synthesis of:

(1) new glasses or ceramic compositions which cannot obtained by conventional processing;

(2) novel phase distributions and/or tailored heterogeneity;

(3) exceptional (chemically) homogeneous and pure materials;

(4) materials with strongly decreased sintering temperature and consequently small grain size;

(5) materials with mixed organic and inorganic functionalities.

The sol–gel process can be divided in two main routes which are shown in fig. 1. In both cases a precursor is hydrolysed while simultaneously condensation/polymerization reactions occur. In the colloidal route the hydrolysis rate is fast by reacting the precursor with excess water and a precipitate of gelatineous hydroxide particles is formed which is peptised in a subsequent step to a stable colloidal suspension. The elementary particle size ranges, depending on the system and the processing, from 3 to 15 nm and these particles form loosely bound agglomerates with sizes ranging from 5 to 100 nm. The size of those agglomerates can be decreased e.g. by ultrasonification of the suspension. By increasing the concentration and/or manipulation of the surface (zeta) potential of the sol particles the suspension is transformed now into a gel structure consisting of interlinked "chains" of particles (see fig. 1). The packing density of such structures can vary from very loose to rather dense depending on the zeta potential. According to Aksay and Schilling [18] colloidal suspensions behave like molecular systems and a phase diagram can be constructed. In the polymeric route the hydrolysis rate is kept low by adding successively small amounts of water. The precursor is partly hydrolysed, OH-groups attached to metal atoms are formed and these hydroxyl groups give rise to condensation reactions yielding a viscous solution of inorganic–organic polymeric molecules. Further condensation/polymerization yield a strongly interlinked gel network, containing a certain percentage of organic material.

In both routes the gels are dried. This is a critical process step which strongly influences the structure of the obtained xerogel particles and its properties (pore size distribution, porosity, internal surface). In most cases the aim is to obtain soft agglomerates which can be packed more efficiently by subsequent application of pressure or can be dispersed again in solution. Finally a heat treatment (calcining or sin-

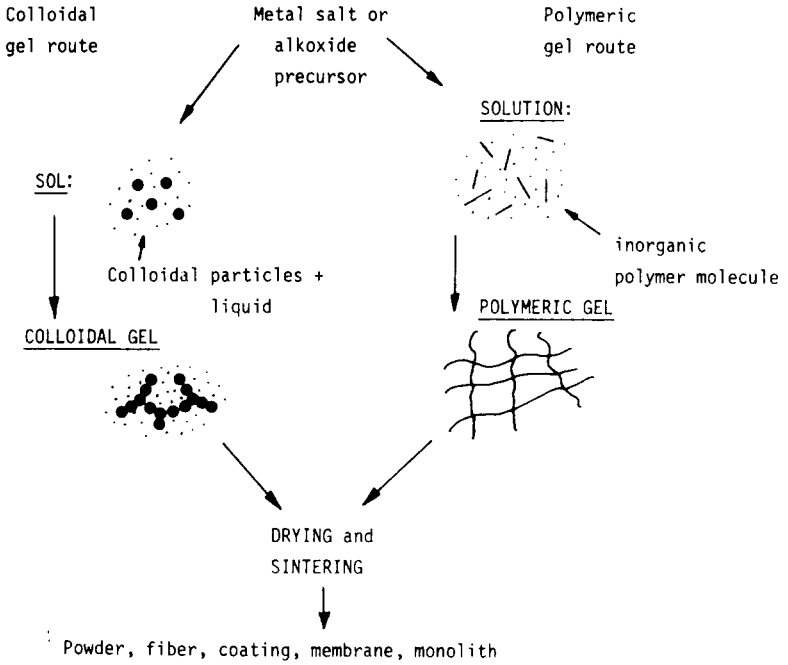

Fig. 1. Scheme of sol–gel routes.

tering) converts the hydroxylated oxide to the final chemically and mechanically stable oxide microstructure.

Binary systems can be obtained e.g. by mixing of sols of different metals [19] or by the cohydrolysis or copolymerization of mixtures of alkoxides [20,21].

To obtain very intimately dispersed (homogenous) mixtures the polymeric gel route seems to be preferable because here the different metal ions in different precursors are linked before they can separate. The ultimate precursor should be then an alkoxide containing two different metal atoms in one precursor molecule. A process coming close to this ideal situation is reported by Morgan et al. [22]. For the Al_2O_3–ZrO_2 system they obtained an ultimately dispersed system.

An interesting method to vary the surface chemistry of particles is to coat them. This is reported by Iler [19] for the production of binary sols of silica and alumina. These coagulate by simple mixing. If the silica sol particles are coated with a 1 nm thick alumina film a homogeneous sol can be obtained. Similar results are reported by Heistand et al. [23] in the synthesis of composite powders of Al_2O_3–TiO_2 and Al_2O_3–ZrO_2. The principle used is shown in fig. 2 and makes use of the hydrolysis of Ti isopropoxide in an alumina dispersion. In the case of TiO_2 coated with alumina, spheroidal particles with a surface area

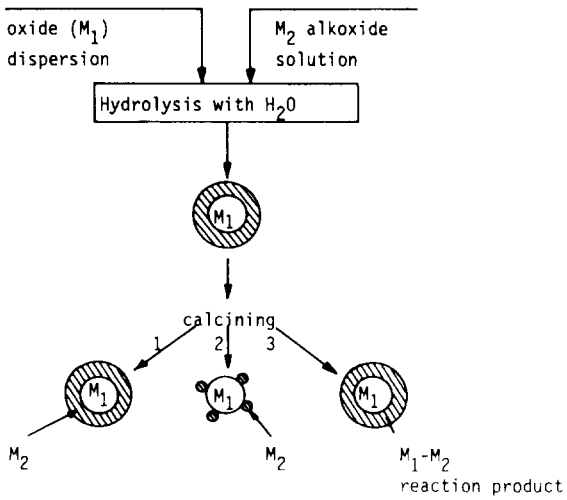

Fig. 2. Schematic representation of composite preparation by a coating procedure.

(S_{BET}) of 190 m^2/g[1] were obtained. In the case of Al_2O_3–ZrO_2, water free alumina dispersed in a solution of Zr tetra-*n*-propoxide in dry alcohol was mixed with a water–alcohol solution. The alkoxide was hydrolyzed now both interstitially and on top of alumina particles. The resulting powder was autoclaved at 250°C (this results in an improved consolidation behaviour). Most of the zirconia particles are attached to alumina particle surfaces and a very finely dispersed duplex type structure is obtained.

In many cases the materials obtained in this way are characterized by the surface area S_{BET} (m^2/g). In the case of dense, spherical particles this surface area can be related to the particle size D by (Ramsay and Avery [24]):

$$S_{BET} = 6/(D^* S_{oxide}) \quad (1)$$

with S_{oxide} is the density (g/m^3) and D, the particle diameter (m). Furthermore the pore size r_p is (linearly) related with D. Using this equation elementary particle sizes ranging from 5 nm or smaller (SiO_2, CeO_2) to 15 nm can be calculated and they are frequently reported with corresponding pore sizes of ≈ 2 nm (SiO_2, CeO_2) to 10 nm. The materials are used for the synthesis of ultra fine grained ceramics, ceramic membranes and catalysts and can be further modified to even finer structures (section 4).

3. Ceramic membranes

Ceramic membranes consist essentially of a porous support of a few millimeter thickness, a porous intermediate layer of 10–100 μm thickness with pores of 0.05–0.5 μm and the proper membrane (separation layer) with a thickness of 1–5 μm. This last layer must have a (very) *sharp* pore distribution and a mean pore size down to 2.5 nm (fig. 3). This separation layer can be further modified (section 4).

They can be made in different ways. The most frequently used methods are slibcasting onto the support system with a sol of the membrane material (which is produced by the colloidal route [25,26,31]) or by film coating with precursor material produced by the polymeric gel route [28,29] (see fig. 1).

During careful drying, capillary forces cause compaction of the gel and a regular packing of particles

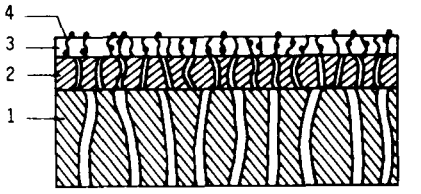

1. porous support (1-15 mu pores)
2. intermediate layer(s) (100-1500 nm)
3. separation (top)layer (3-100 nm)
4. modification of separation layer

1+2 is microfiltration or 'primary' membrane
1+2+3 is ultrafiltration or 'secondary' membrane
1+2+3+4 is hyperfiltration or/and gas separation membrane

Fig. 3. Schematic presentation of a multilayer asymmetric membrane system.

(size 5–10 nm) is formed. Finally calcining transforms the gel material into oxide particles and a stable membrane is formed. An essential feature is that the membrane is crack and defect free. The smaller the elementary particles and the weaker the agglomerates in the sol, the smaller the pore size is and the sharper its distribution will be. Therefore the sol–gel chemistry is an important step.

In this way supported and non-supported toplayers are produced from γ-Al_2O_3, TiO_2, CeO_2, ZrO_2 and binary combinations of them [25,26,30]. Some typical properties are shown in tables 2 and 3. The column temperature and time refers to the calcining temperature and time respectively. The pore diameters are calculated from adsorption–desorption measurements using slit shaped and cylindrically shaped geometries respectively as indicated in the tables. The non-supported membranes have a thickness which can be varied between 20 and 200 μm and have a micro structure which is similar to the supported ones [25,26,35]. The elementary particle shape is important. The most frequently produced membranes consist of alumina. It is produced from plate shape boehmite particles which are packed into a structure represented in fig. 4 as shown by Burggraaf, Keizer and co-workers [25,26]. In the calcining step the boehmite is transformed into an isomorphous γ-alumina layer (temperature 450–650°C) or θ-Al_2O_3 layer (higher temperature). Some characteristic microstructural properties are given in table 4.

Table 2
Structural properties of *non-supported* one-component membranes.

Material	Temperature (h)	Time (°C)	Pore diameter (nm)	Porosity (%)	BET-surface (m^2/g)	Crystal diameter (nm)
γ-AlOOH	34	200	2.5 [a]	41	315	≈5×25(−50) [b]
γ-AlOOH [c]	5	300	5.6 [a]	47	131	≈7×300 [c]
γ-Al_2O_3	34	500	3.2 [a]	50	240	≈5×25(−50)
γ-Al_2O_3 [c]	5	550	6.1 [a]	59	147	≈7×300 [b]
γ-Al_2O_3	34	800	4.8 [a]	50	154	
θ-Al_2O_3	34	900	5.4 [a]	48	99	
α-Al_2O_3	34	1000	78 [d]	41	15	
TiO_2(a)	3	300	3.8 [d]	30	119	sol: 5 [e]
TiO_2(a+r)	3	400	4.6 [d]	30	87	sol: 10–40 [f]
TiO_2(a) [g]	3	450	3.8 [d]	22	80	
TiO_2(a) [g]	3	600	20 [d]	21	10	
CeO_2	3	300	≈2	15	41	
CeO_2	3	400	≈2	5	11	sol: 10(TEM)
CeO_2	3	600	nd	1	1	

[a] Slit shaped pore model. [b] Plate shaped crystals.
[c] Sol prepared at 200°C in autoclave: a=anatase phase; r=rutile phase.
[d] Cylinder shaped pore model. [e] Primary particle (TEM); nd is not detectable.
[f] Agglomerated sol particles (10 nm: use of ultrasonic waves to disperse the agglomerates, laser scattering used as a measuring method).
[g] Titania stabilized with SO_4^{2-} ions.

Table 3
Structural properties of non-supported binary composite membrane system.

Material	Temperature (h)	Time (°C)	Pore diameter (nm)	Porosity (%)	BET-surface (m^2/g)	Crystal diameter (nm)
Al_2O_3/CeO_2 (35 wt%)	3	450	2.4 [c]	39	164	sol: 10 and 50 [b] calc.: 5(CeO_2)
Al_2O_3/CeO_2 (35 wt%)	3	600	2.6	46	133	
Al_2O_3/TiO_2 (30 wt%)	3	450	2.5	48	260	
Al_2O_3/TiO_2 (65 wt%)	3	450	2.5	38	220	
Al_2O_3/ZrO_2 [c]	5	450	2.6	43	216	ZrO_2: nd [d]
Al_2O_3/ZrO_2 [c]	5	750	2.6	44	179	ZrO_2: nd
Al_2O_3/ZrO_2 [c]	5	1000	⩾20			ZrO_2: 10–15

[a] Bimodal distribution of CeO_2 particles. [b] Slit shaped pore model.
[c] 17 wt% ZrO_2. [d] Not detectable, probably ZrO_2 layer on Al_2O_3.

This structure seems to be advantageous to obtain rather easy defect-free structures. With spherically shaped particles it is considerably more difficult to obtain crack-free systems and the processing is much more critical. In the case of γ-Al_2O_3 toplayers the micro structure is build up with penny shaped particles with a size of 25–50 nm (depending on processing) and a thickness of about 3.5–5.5 nm [25,26] (see fig. 6 and table 2). In the case of TiO_2, CeO_2 and ZrO_2 the structure consists of spherically or equi-axed elementary particles with sizes ranging from about 3 nm (CeO_2, which particles easily transform to larger particles), 5–7 nm (TiO_2) or 8–9 nm (ZrO_2) (see table 2).

In the case of the binary systems we have a mixture of plate shaped and spherically shaped particles

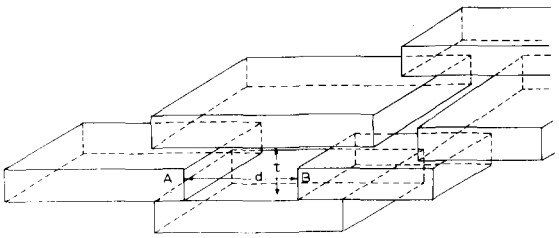

Fig. 4. Model structure of a γ-alumina toplayer.

which form crack-free, mechanically stable layers with characteristics comparable with γ-alumina membranes as long as the volume contribution of the other component is smaller than about 30–40%. See table 3 and compare with table 2 for alumina membranes. Detailed structural investigations are in progress. Some typical TEM pictures are given in fig. 6.

TiO_2 membranes are reported too by Larbot et al. [28] with a very small thickness (0.7 μm) and pore sizes of 5–20 nm. Electronically conductive RuO_2–TiO_2 binary membranes have been synthesized by Guizard et al. [29]. Pore diameters of 10–20 nm were obtained with membranes from colloidal gels and of less than 5 nm for membranes from polymeric gels. No further microstructural details are given.

These systems show all interesting transport and catalytic properties like surface diffusion and improved selectivity and can be used for influencing chemical reactions and separation processes [35,36]. A review has been recently given by Keizer and Burggraaf [32].

4. Modification of membrane structures and surfaces

4.1. Membranes

The membrane (toplayer) structures can be modified further by deposition of material in the internal pore structure from liquids (impregnation, adsorption) or gases. In this case duplex type structures on a scale of 1–2 nm can be obtained. Some results of our current research are summarized in table 5. Several possible situations are schematically shown in fig. 5 and TEM pictures (fig. 6) show the actual situation in some samples from table 5. For silica-based xerogels diphasic nanoscale composites are reported by Komarneni, Roy and co-workers [7]. Typical examples in this case were SiO_2–AgCl, SiO_2–$AlPO_4$, SiO_2–Nd_2O_3 and SiO_2–CdS. In all these cases the second component is the component which is deposited inside the pore structure of the first one. The substructure inside the pores has a characteristic size equal or smaller than the pore size (which is 3–8 nm).

Monolayer techniques are known from catalyst research and are reviewed briefly by Burggraaf and

Table 4
Microstructural characteristics of alumina membranes as a function of sintering temperature and time.

Temperature (°C)	Time (h)	Phase	BET-phase (m^2/g)	Pore diameter (nm)	Porosity (%)
200	34	γ-AlOOH	315	2.5 [a]	41
400	34	γ-Al_2O_3	301	2.7	53
	170	γ-Al_2O_3	276	2.9	53
	850	γ-Al_2O_3	249	3.1	53
500	34	γ-Al_2O_3	240	3.2	54
700	5	γ-Al_2O_3	207	3.2	51
	120	γ-Al_2O_3	159	3.8	51
	930	γ-Al_2O_3	149	4.3	51
800	34	γ-Al_2O_3	154	4.8	55
900	34	θ-Al_2O_3	99	5.4	48
1000	34	α-Al_2O_3	15	78 [b]	41
550 [c]	34	γ-Al_2O_3	147	6.1	59

[a] Slit shaped pore model. [b] Cylinder shaped pore model.
[c] Prepared from a sol treated in an autoclave at 200°C.

Table 5
Some modified nanoscale ceramic microstructures.

Membrane	Deposit	Shape	Loading	Size (nm)
γ-Al_2O_3	Fe or V oxide	monolayer	5–10%	$\approx$0.3 nanometer
γ-Al_2O_3	MgO/MgOH	particles	5–100%	
γ-Al_2O_3	$Al_2O_3/Al(OH)_3$		5–100%	$\approx$5 nanometer
γ-Al_2O_3	Ag	particles	5–50%	> 10 nanometer
γ-Al_2O_3	CuCl/KCl	multilayer		
γ-Al_2O_3	ZrO_2	layers?		
TiO_2	V oxide			
Al_2O_3–TiO_2	V oxide, Ag			
θ/α-Al_2O_3	ZrO_2–Y_2O_3	multi layers, props	1–100%	–few nanometer pore size

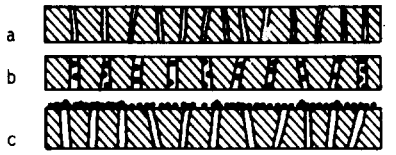

a Homogeneous (multi)layers in the pores
b Plugs in the pores (constrictions)
c Plugs/layers ontop of the pores

Fig. 5. Schematic microstructures of some modified ceramic membrane types.

Gellings [4]. They are applied now by us in membrane systems (table 5 and fig. 5a) using adsorption of metal acetylacetonates from solution, followed by decomposition of the adsorbates. An example is the formation of V oxide monolayers in γ-alumina and binary membranes Table 5). Mg and alumina hydroxides are deposited by a homogeneous precipitation technique inside the pore system and structures and properties are investigated both before and after thermal annealing. In the last case the hydroxides were converted to the corresponding oxides. In both cases crack-free mechanically stable modified membranes (supported and non-supported) could be obtained with locally narrowed (decreased) pore sizes and changed transport properties [39].

Modification along these lines is reported too by Asaeda et al. [33] starting with γ-alumina layers with rather large pores (a few tens of nm) which were subsequently treated by Al isopropoxide and sodium silicate forming an alumina silicate inside the pore system. This system could be used only successfully after thermal treatment in humid air at *low* temperature (90°C).

In our MgO modified systems it could be shown by scanning Auger microscopy (SAM) that a homogeneous distribution of the MgO within the pores and throughout the toplayer (thickness $\approx$3–5 μm) could be obtained. Consequently the MgO substructure has dimensions smaller than 3–5 nm. To obtain a very high loading a specially developed technique has to be used [34]. Electrochemical vapour deposition (ECVD) techniques are used too, to vary the shape and the distribution of the nanoscale deposits in the pore system (table 5, Al_2O_3–(ZrO_2–Y_2O_3) system).

4.2. Ion implantation as a synthesis method

Ion implantation and related ion-mixing processes can be used to change the properties of solid surfaces. A review of the main process parameters, physical processes, applications and possibilities in inorganic and ceramic surfaces has been given by Burggraaf et al. [4].

In the implantation process the surface is bombarded with a beam of high energetic ions (10–500 keV). Due to the penetration of the ions in the material a modified surface layer is formed.

Depending on the process parameters the concentration profile of the dopant ions can be given different shapes, the penetration depth can be varied between some nanometers and about one micrometer and the dopant concentration in the surface can be raised to about 50 at%. This implies that strongly

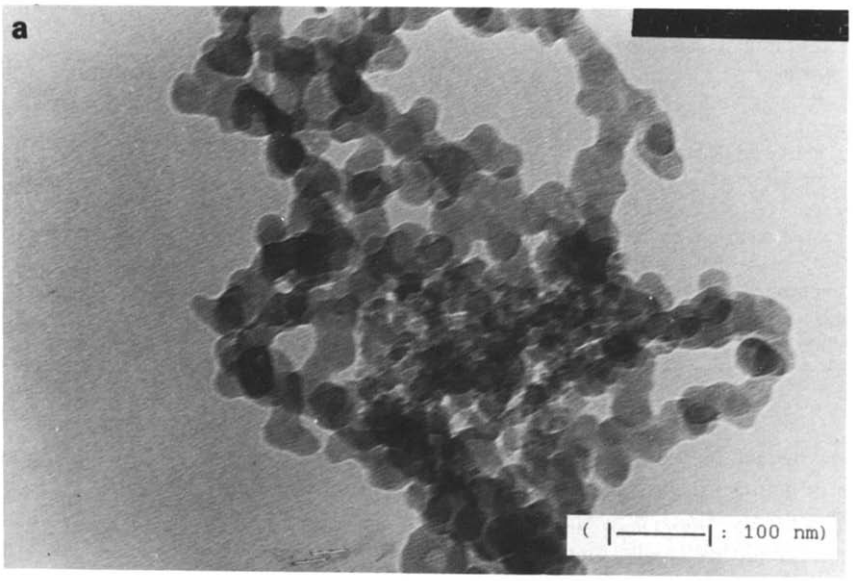

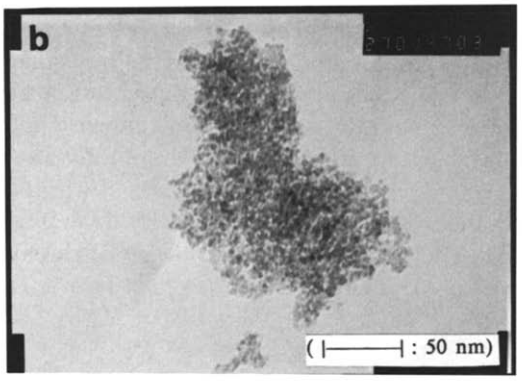

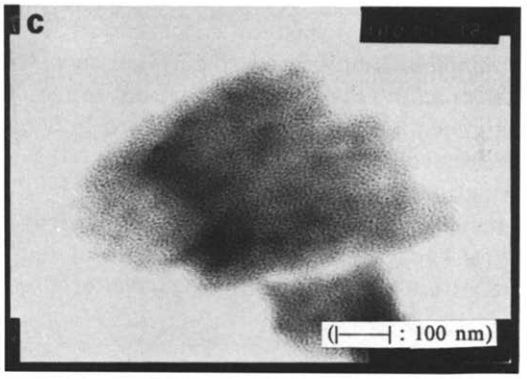

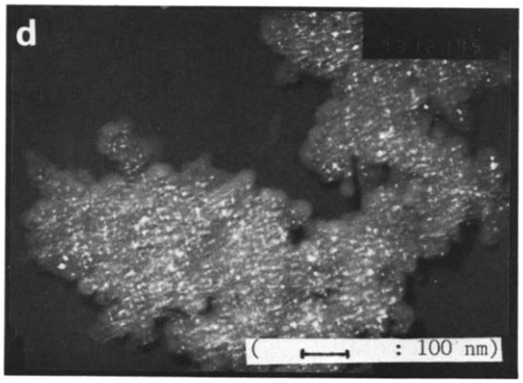

Fig. 6. Typical transmission electron microscopy pictures of some membrane systems: (a) plate shaped boehmite (ALOOH) sol particles, isomorphous with γ-alumina membrane particles; (b) ceria particles in a binary ceria–alumina membrane calcined at 450°C during 5 h; (c) alumina–zirconia membrane (17 wt% zirconia) calcined at 750°C during 5 h; (d) dark-field TEM picture of a Ag-modified γ-alumina calcined at 450°C during 5 h.

Table 6
Chemical effects resulting from implantation. Note: Metastable s.s. and compounds possible.

(I) Reduction/oxidation
different valencies; nonstoichiometry
(II) Bond formation
1. substitutional incorporation of metal ion→*solid solution formation* (s.s.)
2. precipitation of implanted metal ions:
(a) with the matrix→*compound formation*
(b) with each other→*metal cluster formation*, Cermet layer

supersaturated or metastable compositions can be realised. During implantation process the structure of the material is strongly changed by the introduction of lattice defects and this finally can result in the production of an amorphous layer. By subsequent heat treatment (annealing) these defects can be partly removed without changing the concentration profile. A range of chemical effects can result from the implantation process (table 6) and very typical microstructures can be realised, e.g. the formation of microprecipitates (≈ 3 nm) embedded in a metastable supersatured matrix.

An example of this situation is reported by Burggraaf et al. [36] and will be summarised below. The electric and electrochemical properties of implantated oxides are reviewed by Burggraaf et al. [37] and show interesting changes in conductivity and electrochemical activity.

Implantation of ceramic solid solutions of $(1-0,x)ZrO_2$–$(0,x)YO_{1.5}$ with $x=14$–17 (ZY 14–17) with a high dose of Fe result in a microstructure which is summarised in table 7. In the sample code the figures give the amount of implanted ions ($x\times 10^{16}$ at cm^{-2}), the implantation energy (keV) and the annealing temperature (C) respectively.

Initially Fe is present as metallic particles (Fe^0) and as Fe^{2+} and Fe^{3+} ions. A part of the Fe^{3+} ions is dissolved in the ZY matrix (Fe^{3+}) and the remaining Fe^{3+} ions are present in Fe_2O_3 microprecipitates (Fe_h^{3+}). Annealing leads to complete oxidation to Fe^{3+} at low temperature ($\leqslant 400°C$). Transmission electron diffraction/microscopy and Mössbauer spectroscopy show the formation of very small Fe_2O_3 (hematite) particles (<5 nm) which grow after heat treatment at higher temperatures ($>1000°C$). The amount of Fe which can be (metastably) solved in the ZY matrix amounts $\approx 4.5\times 10^{21}$ Fe/cm^3. This is about 3–4 times larger than the equilibrium concentration. Implantation with amounts of Fe$>4.5\times 10^{21}$ Fe/cm^3 results in a dispersion of Fe_2O_3 with nanoscale dimensions in a metastable solid solution of Fe^{3+} in ZY (≈ 5 mol% Fe_2O_3 in ZY).

Similar results have been found for Ti implanted in ZY. The amount of Ti which can be (metastably) solved in the ZY matrix is larger than 16 at% TiO_2.

Table 7
Composition and (nano) structure of iron implanted ZrO_2–Y_2O_3 solid solutions.

Sample code	State of the implanted iron Fe atom (%)					Structure remarks
	Fe	Fe^0	Fe^{2+}	Fe_s^{3+}	Fe_h^{3+}	
as-implanted:						
8–110		55	29	16	34	amorphous (RBS)
8–15	27	14	25		74	microcryst. 30 nm
2–15			26			
annealed:						
8–110–400				41	59	amorphous (RBS)
8–15–400				39	61	
2–15–400				56	44	
2–15–1100				57	43	
8–110–800						amorphous (RBS)
ZYFe10				100		

A maximum concentration of about 70 at% TiO_2 could be obtained in the implanted concentration profile. Consequently it is expected that a dispersion of TiO_2 (with nanoscale dimensions) has been formed. This is investigated now.

In these cases use can be made of nucleation-controlled microstructure development by a two-step heat treatment. In this way Legg [38] obtained interesting microstructures by precipitation of Al_2O_3 in ion-implanted ZY.

5. Conclusions

Powders as well as ceramic membranes and layers can be made with an elementary building unit of the microstructure (crystal diameter, domain) ranging from 2 to 100 nm.

Ceramic membranes having a sharp pore size distribution with a mean pore diameter of 3, 0 nanometer can be made of γ-Al_2O_3, TiO_2, ZrO_2 and CeO_2 and of binary mixtures of them.

The membrane pore structure has been further modified in several ways with e.g. Fe, V, Al or Mg hydroxide or oxide or with metals like Ag or with salts.

The pore size is decreased in this way as well as the chemical character of the system.

Ceramic membrane systems can be used for gas and liquid separation and for influencing chemical reactions. Combination of typical transport properties and catalytic activity can lead to enhanced selectivity and yield, and to a very good control of the residence time.

References

[1] R. Birringer, H. Hahn, H. Höffler, J. Karch and H. Gleiter, Defect Diffus. Forum 59 (1988) 17.

[2] H. Yanagida and Y. Nakamura, New Mater. New Proc. 3 (1985) 13.

[3] H.A. Bender, R.P. Ingel, W.J. McDonough and J.R. Spann, Adv. Ceram. Mater. 1 (1986) 137.

[4] A.J. Burggraaf, P.J. Gellings and D. Scholten, in: High tech ceramics, ed. P. Vincenzini (Elsevier, Amsterdam, 1987) pp. 779–792.

[5] A.F. Leenaars, K. Keizer and A.J. Burggraaf, in: Reverse osmosis and ultrafiltration, eds. S. Sourirayan and T. Matsura, ACS Symp. Series 281 (1987) 83.

[6] K. Keizer and A.J. Burggraaf, Sci. Ceram. 14 (1987) 83.

[7] S. Komarneni, E. Breval and R. Roy, J. Mat. Sci. 21 (1986) 737.

[8] J. Hurt and D.J. Viechnicki, Ultra fine grained ceramics, eds. J. Burke, N.L. Reed and V. Weiss (Syracuse Univ. Press, Syracuse, 1968) pp. 273–293.

[9] C.G.F. Stenger and A.J. Burggraaf, Phys. Status Solidi (a) 61 (1980) 275, 653.

[10] C.A. Randall, D.J. Barker, R.W. Whatmore and P. Groves, J. Mat. Sci. 21 (1986) 4456.

[11] M.P. van Dijk, F.C. Mylhoff and A.J. Burggraaf, J. Solid State Chem. 62 (1986) 377.

[12] B.A. Bender, R.P. Ingel, W.J. McDonough and J.R. Spann, Adv. Ceram. Mater. 1 (1986) 137.

[13] G. Kalonji, J. McKillick and L.W. Hobbs: Adv. Ceram. 12 (1984) 816.

[14] L.L. Hench and D.R. Uhlrich, eds., Ultrastructure processing of glasses and composites (Wiley, New York, 1986).

[15] L.L. Hench and D.R. Uhlrich eds., in: Science of ceramic chemical processing (Wiley, New York, 1986).

[16] C.J. Brinker, D.E. Clark and D.R. Uhlrich, eds., in: Mater. Res. Soc. Symp. Proc. 32 (1984).

[17] R.W. Davidge, ed. in: Novel Ceramic Fabrication Processes, Brit. Ceram. Proc. 38 (1986).

[18] J.A. Aksay and C.H. Shilling, in: Ultrastructure processing of glasses and composites, eds. L.L. Hench and D.R. Uhlrich (Wiley, New York, 1986) ch 34, pp. 439–448.

[19] R.K. Iler, in: Science of ceramic chemical processing, eds. L.L. Hench and D.R. Uhlrich (Wiley, New York, 1986) pp. 3–20.

[20] P.A. Bruggen and A. Mocellin, J. Mater. Sci. 21 (1986) 4431.

[21] E.A. Pugar and P.D. Morgan, J. Am. Ceram. Soc. 69 (1986) C 120.

[22] P.E.D. Morgan, H.A. Bump, E.A. Puigar and J.J. Ralls, Science of ceramic chemical processing, eds. L.L. Hench and D.R. Uhlrich (Wiley, New York, 1986) pp. 327–334.

[23] R.H. Heistand, Y. Oguri, H. Okamura, W.C. Moffat, B. Novick, E.A. Barringer and H.K. Bowen, Science of ceramic chemical processing, eds. L.L. Hench and D.R. Uhlrich (Wiley, New York, 1986) pp. 482–496.

[24] J.D.F. Ramsay and R.G. Avery, Brit. Ceram. Proc. 38 (1986) 275.

[25] A.F.M. Leenaars, K. Keizer and A.J. Burggraaf, J. Mater. Sci. 19 (1984) 1077.

[26] A.F.M. Leenaars and A.J. Burggraaf, J. Colloid Interface Sci. 105 (1985) 27.

[27] A.F.M. Leenaars and A.J. Burggraaf, J. Membrane Sci. 24 (1985) 245, 260.

[28] A. Larbot, J. Alary, C. Guizard, J.P. Fabree, N. Idrissi and L. Cot, in: High tech ceramics, ed. P. Vincenzini, Mater. Sci. Monographs 38 (1987) 2259.

[29] C. Guizard, N. Idrissi, A. Larbot and L. Cot, Brit. Ceram. Proc. 38 (1986) 263.

[30] R.J.R. Uhlhorn, M.H.B.J. Huis in 't Veld, K. Keizer and A.J. Burggraaf, Sci. Ceram. 14 (1987) 551.

[31] R.J. van Vuren, B.C. Bonekamp, K. Keizer, R.J.R. Uhlhorn, H.J. Veringa and A.J. Burggraaf, in: High tech. ceramics, ed. P. Vincenzini, Mater. Sci. Monographs 38 (1987) 2235.

[32] K. Keizer, R.J.R. Uhlhorn, R.J. van Vuren and A.J. Burggraaf, J. Membrane Sci. 39 (1988) 285.
[33] M. Asaeda, Lung Dui Du and M. Fuji, J. Chem. Eng. Japan 19 (1986) 73, 84.
[34] R.J.R. Uhlhorn, K. Keizer and A.J. Burggraaf, ACS Symp. Series (1988), to be published.
[35] V. Zaspalis, K. Keizer, J.G. van Ommen, J.R.H. Ross and A.J. Burggraaf, to be published.
[36] A.J. Burggraaf, D. Scholten and B.A. van Hassel, Nucl. Instr. Methods, in Phys. Res. B 32 (1988) 32.
[37] A.J. Burggraaf and B.A. van Hassel, to be published.
[38] K.O. Legg, J.K. Cochran, H.F. Solnick-Legg and L. Mann, Nucl. Instr. Methods B 7/8 (1985) 535.
[39] R.J.R. Uhlhorn, M. Huis in 't Veld, K. Keizer, A.J. Burggraaf, J. Mater. Sci., to be published.